

Phase Diagram of Iron by in Situ X-ray Diffraction: Implications for Earth's Core

C. S. Yoo,* J. Akella, A. J. Campbell,† H. K. Mao, R. J. Hemley

The phase diagram of iron has been studied to 130 gigapascals (1 gigapascal = 10^4 atmospheres) and 3500 kelvin by a combined laser-heated diamond-anvil cell and x-ray diffraction technique that provides direct identification of the solid phases. Iron in the hexagonal close-packed (hcp) phase (ϵ -Fe) is stable from 50 to at least 110 gigapascals at high temperatures. The wide stability field of ϵ -Fe indicates that this polymorph should currently be considered the most relevant solid phase for Earth's core. The triple point between the γ , ϵ , and liquid phases is located at 2500 ± 200 kelvin and 50 ± 10 gigapascals. There is evidence for a phase with a double hcp structure below 40 gigapascals and for another transition above 110 gigapascals and 3000 kelvin.

Because iron is the dominant component of Earth's core, information on the behavior of iron at high pressures and temperatures is fundamental to Earth science. In particular, determination of the phase diagram of iron is central to understanding a number of properties and processes of the planet's deep interior, including the temperature profile, chemical composition, energy balance, dynamics, and geomagnetism (1–4). High-pressure diamond-anvil cell (5–7) and shock-wave experiments (7–10) are providing important constraints on the phase relations over a growing range of pressure and temperature. However, the accurate determination of the phase diagram of this crucial element under Earth-core conditions is still a formidable experimental problem because of the extreme pressure and temperature (P - T) conditions involved.

Five phases of iron, namely α [body-centered cubic (bcc)], γ [face-centered cubic (fcc)], δ (bcc), ϵ (hcp), and β (no structural information), have been reported. Crystal structures and phase boundaries of α -, γ -, δ -, and ϵ -Fe are well determined at low pressures (below 20 GPa). As indicated by x-ray diffraction measured to 300 GPa at ambient temperature, ϵ -Fe is the stable phase of iron at 300 K to pressures of Earth's core (11). Phase boundaries at high temperatures and pressures, however, have been determined primarily by indirect methods. Because these do not provide unequivocal identification of solid phases, several key aspects of the phase diagram are uncertain. First, the location of the ϵ - γ -liquid triple point is not well established (1, 5, 12, 13). Second, various determinations of the melting temperature above 50 GPa are discrep-

ant; this includes differences among the static measurements (5–7) and between static and shock-wave results (7–10). Third, the structure and stability field of the β phase remain to be clarified. Fourth, the nature of the 200-GPa transition suggested by shock-wave experiments is unknown (10). A reentrant α' (bcc) phase (2) or the β phase (5, 6) was proposed to explain the transition; however, subsequent theoretical calculations indicated that the bcc structure is mechanically unstable under these conditions (3, 14).

We developed an integrated diamond-anvil cell, x-ray, and laser-heating technique to examine the iron phase diagram by directly probing the crystal structure of the phases in situ at high temperatures and pressures. This system consists of three components (15): (i) a Nd-yttrium-aluminum-garnet laser-heating system to heat the sample in a diamond-anvil cell, (ii) a microscope system to measure temperature and view the sample for alignment and direct observation, and (iii) a synchrotron x-ray and energy-dispersive diffraction system. A small piece of thin iron foil is loaded in a diamond cell, together with a pressure medium such as argon, Al_2O_3 , or LiF. Polychromatic (white) x-ray radiation from the synchrotron source is coaxially aligned to the center of laser heating spot, and the diffraction from the sample is recorded at a fixed scattering angle 2θ as a function of energy. The temperature of the sample is simultaneously determined from the thermal emission from the laser-heated area. The pressure of the sample is determined either by the equation of state of the sample or from the ruby luminescence method (16).

There was a distinct change in the x-ray diffraction pattern of iron upon melting during laser heating. For example, at 50 GPa (Fig. 1) at least four strong features from ϵ -Fe and several weak bands from Al_2O_3 were observed at 300 K. During laser heating to 2280 K, all of the diffraction

lines of ϵ -Fe shifted to lower energies or higher d spacings, indicating thermal expansion of the iron. There was little change in the relative intensity of the iron diffraction pattern in comparison to that of Al_2O_3 , and thermal broadening of the diffraction bands was negligible. Near 2580 K, however, the diffraction lines of ϵ -Fe weakened and disappeared, indicating that the sample in the laser-heated spot had melted. Upon cooling, each of the diffraction lines of ϵ -Fe reappeared (Fig. 1, top curve). The quenched ϵ -Fe crystallized with preferred orientation of the (100) plane in the diffraction direction. After heating, a small circular trace was evident visually in the laser-heated area, providing further indication of melting. These measurements also bracketed the melting temperature at this pressure between 2280 and 2580 K.

At 50 GPa, we observed ϵ -Fe up to 2480 K and conclude that the melting temperature is 2530 ± 50 K. This value is consistent with results reported in (5). The ϵ -Fe is the only solid phase observed up to at least 110 GPa. We noticed during laser heating at 96 GPa (Fig. 2) that the diffraction peaks shifted and changed in intensity, particularly the 101, 110, and 112 reflections. All of the features can be understood in terms of ϵ -Fe and Al_2O_3 , and no new features developed at high temperatures. The above measurements indicate that between 50 to 110 GPa, ϵ -Fe is the stable solid phase at least to the melting curve proposed in (5).

There were indications of a transition at higher pressures (above 110 GPa) and higher temperatures. Diffraction peaks charac-

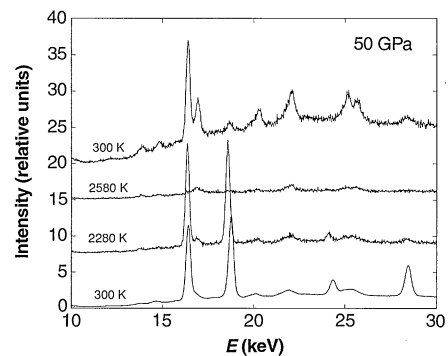


Fig. 1. The x-ray diffraction patterns of the laser-heated iron at 50 GPa, showing the melting of iron at 2580 K. Starting at 300 K (bottom curve; divided by 50 for clarity), the sample was heated through 2280 K to 2580 K, and then cooled back to 300 K (top curve; multiplied by 3). The ϵ phase is evident from four strong features—the 100 diffraction peak at 16.44 keV, 101 at 18.78 keV, 102 at 24.36 keV, and 110 at 28.48 keV—and a weaker feature of the 200 peak at 17.80 keV ($Ed = 33.94$ keV Å, where E is energy and d is the d spacing). The iron melted from the ϵ phase, suggesting that the γ - ϵ -liquid triple point is located in the vicinity of this pressure.

C. S. Yoo and J. Akella, Lawrence Livermore National Laboratory, University of California, Livermore, CA 94551, USA.

A. J. Campbell, H. K. Mao, R. J. Hemley, Geophysical Laboratory and Center for High Pressure Research, Carnegie Institute, Washington, DC 20015, USA.

*To whom correspondence should be addressed.

†Present address: G.E. Superabrasives, 6325 Huntley Road, P.O. Box 568, Worthington, OH 43085, USA.

teristic of the ϵ phase were observed below 2500 K at 125 GPa (Fig. 3), but these diffraction lines weakened significantly above 2500 K and eventually disappeared above 3300 K. Moreover, a new line developed at 15.22 keV ($d = 2.229 \text{ \AA}$) above 2920 K, where the diffraction lines of ϵ -Fe disappeared. The new band was not associated with Al_2O_3 but arose from the iron portion of the sample. In addition, the 104 and 110 lines of Al_2O_3 should have been located at 14.62 keV ($d = 2.321 \text{ \AA}$) and 15.68 keV ($d = 2.164 \text{ \AA}$), respectively, at this pressure (17). We were able to quench the new diffraction band at ambient temperature after heating. The iron sample quenched from 3300 K showed no relation to the ϵ phase; in addition, there was little change in visual appearance of the sample.

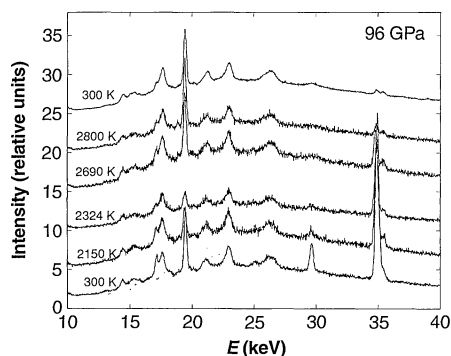


Fig. 2. The x-ray diffraction patterns of the laser-heated iron at 96 GPa, showing that β -Fe is not evident to 2800 K at this pressure. The heating cycle starts with the bottom curve and moves upward. The ϵ phase is evident at all of the temperatures by the 100, 101, 102, 110, and 112 bands at, respectively, 17.15, 19.46, 25.10, 29.64, and 34.97 keV ($Ed = 33.94 \text{ keV \AA}$). Other, weaker broad features are from Al_2O_3 . Also noticed is the recrystallization of ϵ -Fe above 2300 K.

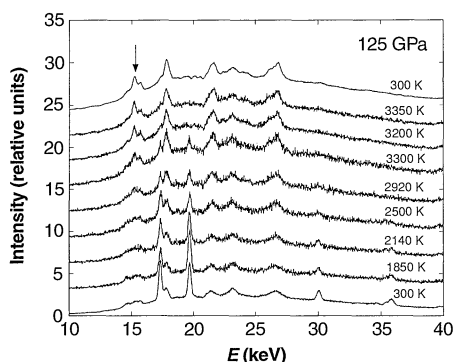


Fig. 3. The x-ray diffraction patterns of the laser-heated iron at 125 GPa, showing that a new diffraction line (arrow) develops as the diffraction lines from ϵ -Fe disappear above 3000 K. The 100, 101, 110, and 112 reflections of ϵ -Fe are located at 17.33, 19.71, 30.07, and 35.81 keV, respectively ($Ed = 33.94 \text{ keV \AA}$). The heating cycle starts with the bottom curve and moves upward.

We conclude that the loss of the diffraction intensity of ϵ -Fe was not a result of melting but instead arose either from a previously undisclosed high P - T solid-solid transition or from a reaction between Fe and Al_2O_3 (18). The transition temperature was close to that previously reported for melting at this pressure (5). It is therefore possible that these observations refer to the same transition, although our current understanding of the transition is too premature to completely rule out alternative hypotheses.

The P - T conditions of the present measurements are compared in Fig. 4 with phase boundaries taken from the literature. Between 50 and 110 GPa, only the hcp diffraction pattern is observed. These results contrast with the previously suggested stability field of β -Fe. The β phase was originally suggested on the basis of an abrupt change in either the laser power or the reflected light intensity as a function of the sample temperature during laser heating (5, 6). Such change does not necessarily reflect a structural phase transition; it could also be caused by electronic transitions or even by mechanisms unrelated to phase transitions (19).

Our results also provide information on the phase diagram at lower pressures. Between 15 and 40 GPa at moderate temperatures, we found a phase of iron that yields a diffraction pattern that can be indexed as a double hcp (dhcp) structure, that is, with an ABAC stacking sequence (20). The dhcp phase has also been observed in a recent study below 40 GPa (21). Our measurements indicate that from 40 GPa to between 110 and 150 GPa, the dhcp phase is not observed

in most of the previously suggested β -Fe field (5, 6). This phase, which we tentatively called ϵ' -Fe, was observed mostly in a portion of stability field previously assigned for γ -Fe, and a small corner of the field for β -Fe. The γ -phase was observed at higher temperatures than the ϵ' -phase to 50 GPa, but not at higher pressures. These results indicate that γ -Fe and ϵ' -Fe are lower pressure phases and thus are not relevant to the core (135 to 363 GPa).

In summary (Fig. 4), our results indicate that the line between the γ or ϵ' phases and the ϵ phase should be either straight or concave up (22). Considering that the melting temperature determined here agrees with values reported earlier (5, 6), one can extrapolate the $\gamma(\epsilon')$ - ϵ phase line to the melting line in Fig. 4. This indicates that the ϵ - γ -liquid triple point is at $2500 \pm 200 \text{ K}$ and $50 \pm 10 \text{ GPa}$, substantially lower than 100 GPa. Above 50 GPa, we observed neither the ϵ' phase nor any diffraction lines that could be indicative of other new phases (for example, β - or α -Fe). Only the ϵ phase is evident between 50 and 110 GPa, in a wide range of temperatures at least to the melting line reported in (5). Above 100 to 120 GPa, however, the nature of the iron phase diagram is not well established (Fig. 3). We conjecture that either a new solid-solid transition or more likely a chemical reaction occurs above 110 GPa and 3000 K in Fig. 4. In this case, the actual melting temperatures of iron at these pressures could be substantially higher than those reported in (5).

REFERENCES AND NOTES

- O. L. Anderson, *J. Geophys. Res.* **95**, 21697 (1990).
- M. Ross, D. A. Young, R. Grover, *ibid.*, p. 21713.
- J. Moriarty, in *High Pressure Science and Technology-1993*, S. C. Schmidt *et al.*, Eds. (American Institute of Physics, New York, 1994), p. 233; R. E. Cohen *et al.*, *ibid.*, p. 891.
- L. Stixrude and R. E. Cohen, *Science* **267**, 1972 (1995).
- R. Boehler, *Nature* **363**, 534 (1993); _____, N. von Bargen, A. Chopelas, *J. Geophys. Res.* **95**, 21731 (1990).
- S. K. Saxena, G. Shen, P. Lazor, *Science* **260**, 1312 (1993); *ibid.* **264**, 405 (1994).
- Q. Williams *et al.*, *ibid.* **236**, 181 (1987).
- C. S. Yoo, N. C. Holmes, M. Ross, D. J. Webb, C. Pike, *Phys. Rev. Lett.* **70**, 3931 (1993).
- K. G. Gallagher and T. J. Ahrens, *Eos* **75** (fall suppl.), 653 (1994).
- J. M. Brown and R. G. McQueen, *J. Geophys. Res.* **91**, 7485 (1986). Two transitions of iron were reported in this work: a solid-solid transition at 200 GPa and melting at 240 GPa. The transition temperatures were calculated to be $4400 \pm 400 \text{ K}$ at 200 GPa and $5300 \pm 400 \text{ K}$ at 240 GPa.
- H. K. Mao, Y. Wu, L. C. Chen, J. F. Shu, A. P. Jephcoat, *J. Geophys. Res.* **95**, 21737 (1990).
- R. Boehler *et al.*, *J. Appl. Phys.* **65**, 1795 (1989).
- H. K. Mao, P. M. Bell, C. Hadjidiacos, in *High Pressure Research in Mineral Physics*, M. H. Manghnan and Y. Syono, Eds. (American Geophysical Union, Washington, DC, 1987), p. 135.
- W. A. Bassett and M. S. Weathers, *J. Geophys. Res.* **95**, 21709 (1990).
- The technique used synchrotron x-ray radiation from beamline X17C of the National Synchrotron Light

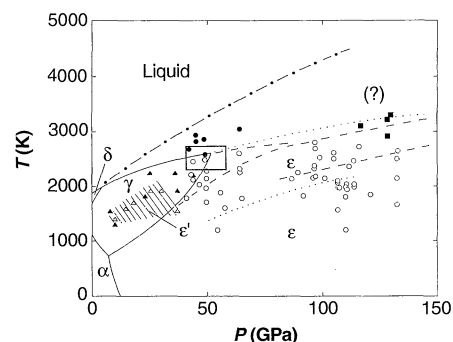


Fig. 4. Constraints for the phase diagram of iron. Various symbols indicate the phases of iron as determined by in situ x-ray diffraction at high pressures and temperatures: liquid iron (●), ϵ -Fe (○), ϵ' -Fe (△), γ -Fe (▲), and new crystalline (■). The area indicated by the large rectangle constrains the location of the ϵ - γ -liquid triple point. The hatched area indicates the P - T region of which the ϵ' phase forms between 15 and 40 GPa. Previously reported phase boundaries are also reproduced for comparison: melting lines are reproduced from (5) (upper dashed line), from (6) (upper dotted line), and from (7) (dashed-dotted line), and ϵ - β boundaries are shown from (5) (lower dashed line) and from (6) (lower dotted line).

Source and a laser-heating system similar to one reported previously [C. S. Yoo *et al.*, *Phys. Rev. B* **48**, 15529 (1993)]. The x-ray beam size, 20 μm by 20 μm , was comparable to the size of laser-heating spot, which varied from 30 to 100 μm , depending on the temperature. (For the later part of this study, we reduced the size of x-ray beam to 5 μm by 20 μm by focusing the 75 μm by 20 μm beam in the vertical direction with an x-ray focusing reflector.) Therefore, the temperature gradients could be large in both the radial and axial directions of the sample being x-rayed; we estimated that this could be as much as 10% of the value reported here. The x-ray diffraction of iron was collected at $2\theta = 19^\circ$ or 21° for 1 to 10 min to obtain the spectra presented here. The microscope system contains an achromatic objective lens that can cause some chromatic aberration and, thereby, the uncertainty in temperature. This uncertainty could be significant in the case where the temperature is measured from a heating spot smaller than a few to several micrometers. However, considering the relatively large heating spot used in this study, we estimate that it is a minor effect. The details regarding the setup will be presented elsewhere [C. S. Yoo *et al.*, in preparation].

16. H. K. Mao *et al.*, *J. Appl. Phys.* **49**, 3276 (1978).
17. A. P. Jephcoat, R. J. Hemley, H. K. Mao, *Physica B* **150**, 115 (1988).
18. The d spacing of the new diffraction line, 2.229 \AA , is close to the 100 peak of the NiAs structure of FeO found at 96 GPa and 800 K [Y. Fei and H.-K. Mao, *Science* **266**, 1678 (1994)], which could suggest that a new chemical reaction occurs at megabar pressures.
19. For example, the observed recrystallization of ϵ -Fe at 2320 K (Fig. 2) is close to the previously reported ϵ - β boundary (5, 6). The change of texture could conceivably alter the nature of light reflection or absorption and give rise to the previously observed effect.
20. The ϵ' -Fe phase was found at temperatures below those of γ -Fe and at pressures between 15 and 40 GPa. At 30 GPa, the volume of ϵ' -Fe is about 6.111 cm^3/mol , which lies between those of ϵ -Fe (5.976 cm^3/mol) and γ -Fe (6.298 cm^3/mol) [C. S. Yoo *et al.*, in preparation].
21. S. K. Saxena *et al.*, *Science* **269**, 1703 (1995).
22. For convenience, we refer to the γ - ϵ phase line as the $\gamma(\epsilon')$ - ϵ line. There are two constraints for the $\gamma(\epsilon')$ - ϵ phase line. First, the resistivity measurements of iron at low pressures constrain the γ - ϵ phase line

below 20 GPa (13). Second, the present study shows that the ϵ - γ -liquid triple point is located at the vicinity of 50 GPa. To satisfy these two conditions, the ϵ - γ phase line cannot be concave down as presented in (5) and should be either concave up or at least straight. However, considering the existence of ϵ' -Fe and the magnetic properties of γ -Fe and ϵ' -Fe (20), the exact nature of the γ - ϵ phase line could be substantially more complicated.

23. We thank C. Ruddle and J. Hu for experimental assistance, B. Goodwin and C. Mailhot for support, and C. Meade, N. C. Holmes, W. J. Nellis, and M. Ross for discussions. Work at Lawrence Livermore National Laboratory (LLNL) was supported by the Laboratory Directed Research and Development Program grant LDRD 94-SR-042 and a Defense Program and was performed under the auspices of the U.S. Department of Energy (DOE) by LLNL under contract W-7405-ENG-48. Research at the Geophysical Lab and the National Synchrotron Light Source (NSLS) was supported by the National Science Foundation; NSLS is supported by DOE.

20 June 1995; accepted 25 August 1995

Expansion of SN 1993J

J. M. Marcaide,* A. Alberdi, E. Ros, P. Diamond, I. I. Shapiro, J. C. Guirado, D. L. Jones, T. P. Krichbaum, F. Mantovani, R. A. Preston, A. Rius, R. T. Schilizzi, C. Triglio, A. R. Whitney, A. Witzel

A sequence of images from very long baseline interferometry shows that the young radio supernova SN 1993J is expanding with circular symmetry. However, the circularly symmetric images show emission asymmetries. A scenario in which freely expanding supernova ejecta shock mostly isotropic circumstellar material is strongly favored. The sequence of images constitutes the first "movie" of a radio supernova.

The recent discovery (1) by very long baseline interferometry (VLBI) of a shell-like radio structure in SN 1993J in the galaxy M81

offers the opportunity to monitor a supernova expansion in a manner that is free from modeling uncertainties (2, 3). Indeed, the angular resolution limit of VLBI, imposed by the size of the Earth, and the angular size of a supernova, determined by its distance from Earth, have generally not permitted a model-free determination of expansion in a young supernova. The relative proximity of SN 1993J, however, together with its strong centimeter emission, permit a reliable determination of the details of the expansion.

Our observations were carried out from September 1993 through September 1994 (Table 1). Images were obtained at 3.6 cm and 6 cm (Fig. 1). The image from November 1993 is from the discovery of the shell-like structure (1). The image from May 1994 was obtained with a large and well-calibrated array; therefore, all details in it are reliable. However, to obtain the images from September 1993 and February 1994, we used circularly symmetric models of sizes extrapolated and interpolated from the images from November 1993 and May 1994, respectively, as initial models in the mapping process. For the September 1993 image, extrapolation was needed because there was insufficient interferometric resolution to resolve the shell; and

for the February 1994 image, interpolation was needed because there were insufficient data (UV coverage) to reconstruct the image unambiguously without a priori information. The procedure we followed allowed us to reliably compare the sizes of the images obtained from the data at each epoch and thus to obtain the angular size growth rate and to learn how the emission enhancement in the southeastern part of the images evolved with time. The latter question is important in distinguishing which features of the emission correspond to traces of the initial explosion and which are induced by the dynamics of the evolution. In spite of the wavelength difference, the image at 6 cm (Fig. 1) from September 1994 shows a remarkably similar structure to those shown in images obtained at 3.6 cm at earlier epochs. However, comparison of the size of the image from this epoch with those from previous epochs is done with caution, because relevant opacity effects may not be accounted for.

Although the interferometric phases for September 1993 contain key information about the emission asymmetry, the source was not large enough then for us to distinguish shell emission from disk emission even when we used the largest available Earth-sized array: A range of limb-brightened disk-like images, each with a characteristic size, are compatible with these data (image degeneracy) (4). Therefore, to determine the expansion rate without bias, we used the backward-extrapolated image from our November 1993 and May 1994 images in Fig. 1 in the mapping process to break this degeneracy and thus to estimate a size (4).

From observation in February 1994 we have high-quality data, but from only a three-antenna array. The interferometric amplitude data require a shell-like structure, and the interferometric phase data require an emission asymmetry in the shell. Use of a point-like source as an initial model made

J. M. Marcaide and E. Ros, Departamento de Astronomía, Universitat de València, E-46100 Burjassot, València, Spain.

A. Alberdi, Laboratorio de Astrofísica Espacial y Física Fundamental, Instituto Nacional de Técnica Aeroespacial (INTA), E-28080 Madrid, Spain, and Instituto de Astrofísica de Andalucía-Consejo Superior de Investigaciones Científicas (CSIC), Apdo. Correos 3004, E-18080 Granada, Spain.

P. Diamond, National Radio Astronomy Observatory, Socorro, NM 87801, USA.

I. I. Shapiro, Harvard-Smithsonian Center for Astrophysics, Cambridge, MA 02138, USA.

J. C. Guirado, D. L. Jones, R. A. Preston, Jet Propulsion Laboratory, California Institute of Technology, Pasadena, CA 91109, USA.

T. P. Krichbaum and A. Witzel, Max-Planck Institut für Radioastronomie, Auf dem Hügel 69, D-50131 Bonn, Germany.

F. Mantovani, Istituto di Radioastronomia, Consiglio Nazionale delle Ricerche (CNR), I-Bologna 40129, Italy.

A. Rius, Laboratorio de Astrofísica Espacial y Física Fundamental, INTA, E-28080 Madrid, Spain, and Centre d'Estudis Avançats-C.S.I.C., Camí de Santa Barbara s/n, E-17300 Blanes, Girona, Spain.

R. T. Schilizzi, Joint Institute for VLBI in Europe, Postbus 2, 7990 AA Dwingeloo, Netherlands, and Leiden Observatory, Postbus 9513, 2300 RA Leiden, Netherlands.

C. Triglio, Istituto di Radioastronomia, CNR, Noto, Italy.

A. R. Whitney, Massachusetts Institute of Technology-Haystack Observatory, Westford, MA 01886, USA.

*To whom correspondence should be addressed.